International Journal for Multidisciplinary Research (IJFMR)
E-ISSN: 2582-2160 ● Website: www.ijfmr.com ● Email: editor@ijfmr.com

A Comparative Study on Gas-Sensing Behavior of Reduced Graphene Oxide (Rgo) Synthesized by Chemical and Environment-Friendly GreenMethod

Dr. P. Laveena Manjulatha

Asst Prof Of Physics, Department Of Physics, Vivekananda Govt Degree College, Vidyanagar, Ahayderabad, Telangana, India-500044.

Abstract

This paper presents a comparative study on gas-sensing behavior of reduced graphene oxide (rGO) synthesized by chemical and green synthesis route. GO is synthesized by Hummers method and then reduced employing two reducing agents hydrazine hydrate [represented by $(rGO)_1$] and L-citrulline [represented by $(rGO)_2$]. Synthesized products were then obtained in the form of thin films, and tested for 10 ppm NO_2 and CO at operating temperatures of 50, 100, and 150 °C. The green-synthesized reduced graphene oxide $(rGO)_2$ exhibits higher relative response of 254.7% as compared to conventionally synthesized $(rGO)_1$ (93.9%) and GO (22.7%) for 10 ppm NO_2 at operating temperature of 150 °C. Furthermore, a switching of conductivity from usual p-type behavior to n-type on exposure of NO_2 is observed at all operating temperatures (50, 100, and 150 °C) for GO, $(rGO)_1$, and $(rGO)_2$. The XRD, FTIR, and Raman confirm the oxidation and reduction process. $(rGO)_2$ shows high thermal stability as observed through TGA. FESEM and TEM images show wrinkled sheet structure for GO as well $(rGO)_1$ and $(rGO)_2$. The data observed from the characterization of resultant products have made it possible to explain better reduction of GO through green-reducing agent and enhanced gas-sensing performance of green-synthesized reduced graphene oxide.

Keywords Green synthesis · Reduced graphene oxide · L-Citrulline · Gas-sensing application · Environment impact

Introduction

The controlled emission guideline has always been a topic of importance due to the need to protect the environment and the quality of human life. Many gases such as CO, CO_2, NO, and NO_2 are lethal as they produce ozone, smog, and acid rain and various unfavorable effects. A common pol- lutant NO_2 which is one of the NOx derivatives and leads to the formation of smog affects lungs and makes human life complicated to live is an extensively studied gas (Wu et al. 2015). The major contributors to NO_2 emission are coal- fired power stations and manufacturing industries along with the vehicular exhaust. The WHO guidelines (https://www. who.int/news-room/fact-sheets/detail/ambient-(outdoor)-air- quality-and-health) have posted a value of NO_2 exposure as 200 $\mu g/m^3$ (1-h mean) and of CO as 117 mg/m^3 (15 min) for safe exposure of these toxic gases to human beings. The concentration of NO_2 and CO could rise to a harmful level in confined spaces such as under the bridges, inside tun- nels, and heart disease. Therefore, the development of small, cheap, reliable, and low-power consuming gas sensors is necessary to protect human beings from excessive exposure to NO_2 and CO toxic gases.

A gas sensor is a device that can detect the presence/concentration of combustible, flammable, and toxic gases (NO_2, CO, H_2, CH_4, NH_3, H_2S, ethanol, etc.) in a given area. The development of gas sensors was contributed immensely by a variety of semiconducting metal oxides (SMOs) such as SnO_2 (Xue et al. 2017), ZnO (Zhezhe et al. 2017), Fe_2O_3 (Dai et al. 2017), etc. in various structural forms, viz., nanowires, nanotubes, and nanoparticles. The driving force for these many investigations lies in their processibility, high sensitivity, and fast response time of these sensors. How- ever, they exhibit some bottlenecks in terms of short life, high operating temperature, and poor selectivity (Yang et al. 2017).

Above problems have been overcome using carbon mate- rials and their composites with metal oxides as reported by Zhang et al. (Jin et al. 2018) and Que et al. (Gong et al. 2010). In view of the above, the sear- ch of novel materials is viable which can show better capabilities for gas sensors.

It has been proved theoretically and experimentally (Tian et al. 2018) that graphene and its derivatives (GO/rGO) are promising candidates for detection of gases as CO, H_2, NO_2, NH_3, etc. due to their unique properties like high electron mobility, excellent conductivity, mechanical strength, high surface area, and easy adsorption of gas molecules (Robin- son et al. 2008). Furthermore, graphene-based devices have low 1/f noise and Johnson noise due to their low crystal defect density and high conductance, respectively (Zhou et al. 2014). Its planar nanostructure makes its suitable for device integration (Yoon et al. 2011). Recent studies have also reflected graphene as a suitable material for research with a wide range of applications including sensor (Liu et al. 2012), super capacitor (Sweet 2015), catalysis (Huang et al. 2012), and thin-film transistors (Eda et al. 2008) because of its high carrier mobility (Zhang et al. 2005), surface area (Singh et al. 2011), and thermal conductivity (Singh et al. 2011). All these studies have led to a better understanding of structure and structure–property correlation for tunability. One of the derivatives of graphene, reduced graphene oxide (rGO), contains many dangling oxygen atoms which act as binding sites for gas analytes and make it a candid material for gas-sensing studies (Zhou et al. 2014).Chemical method is a versatile, easy, and scalable method for GO production and its further reduction to rGO in bulk at low cost. Chemically synthesized rGO can be used for energy storage and many other electronic devices, but the reducing agents used for reduction like hydrazine hydrate (Dave et al. 2015) and sodium borohydrate (Dave et al. 2015) are harmful to the environment and produces health issues (Bo et al. 2014). Use of hydrazine hydrate, sodium boro hydrate, and their derivatives removes epoxide, hydroxyl, and other oxygen functional groups from GO, but during reduction, emission of harmful gases takes place which poses a risk for human health; so to overcome this, attention has been focused on development of eco-friendly synthesis method for the production of rGO and then tested for sensing of CO and NO_2 gas. To the best of our findings, there are very few reports (Chen et al. 2016; Wang et al. 2017; Ye et al. 2017) on the reduction of GO by green-reducing agents. Green- reducing agent L-glutathione was used by Pham et al. (Anh et al. 2011) for the synthesis of graphene nanosheets for electronic devices. Wang et al. (2017) have used green- reducing agent alanine to reduce GO for the production of biomaterial. In other reports, L. Valine and Vitamin C were used by Aunkor et al. (Online et al. 2016) and Fernández-Merino et al. (2010), respectively, for success- ful reduction of GO to alleviate the environmental issues. Some rGO-based materials have been earlier used for detection of CO and NO_2 gases such as rGO using hydrazine hydrate (Liu et al. 2014), cysteamine (Su and Shieh 2014), and caffeic acid (Bo et al. 2014). Inspired by the successful use of green-reducing agents, in the current manuscript, a green-reducing agent L-citrulline was employed to produce rGO and a comparative study was then performed on the relative NO_2- and CO-sensing capabilities of p-type GO (synthesized using Hummer's method), reduced graphene oxide synthesized using hydra- zine hydrate $(rGO)_1$, and L-citrulline $(rGO)_2$ at operating temperatures of 50 °C, 100 °C, and 150 °C. It is observed in the present study that green-synthesized reduced gra- phene oxide $(rGO)_2$ is able to detect

an optimum concen- tration of NO_2 with higher relative sensitivity than hydra- zine hydrate reduced graphene oxide $(rGO)_1$ at 150 °C. A deviation from usual p-type conductivity to n-type is also observed when NO_2 gas flows on all three specimens [GO, $(rGO)_1$, and $(rGO)_2$] at all operating temperatures. Such abnormal behavior on NO_2 exposure has been primarily reported for metal oxide (Vyas et al. 2013) which requires small grain size, lower bulk donor density, and higher den- sity of surface acceptor states. These all conditions make the metal-oxide grain depleted of charge carriers and help in formation of an inversion layer (Sberveglieri 2008). The possible cause of such behavior in GO, $(rGO)_1$ and $(rGO)_2$ is explored the results obtained from the analytical tech-niques used.

Experimental section

The necessary chemicals, graphite fine powder (99.5%, 150 mesh), potassium permanganate (99%), and sodium hydroxide pellets were purchased from CDH, while sul- phuric acid (98%), hydrogen peroxide (30%), hydrazine hydrate (98%), and L-citrulline (99.9%) were purchased from Rankem. Hydrogen chloride (12 N) and ethylene gly- col (99%) were purchased from Merck. These chemicals were used without further purification. Hummer's method (Sharma et al. 2017b) was used for the synthesis of GO powder.

Reduction of GO using hydrazine hydrate $(rGO)_1$

Synthesized GO (500 mg) was added into 200 mL DI (de- ionized) water and sonicated for 3 h until GO flakes were well dispersed. Hydrazine hydrate (2 mL of 100 mM) was added into the well-dispersed GO solution and stirred for 2 h at 80 °C. The mixture was cooled down at RT and washed with NaOH (1 M, it is also useful for reduction of remaining carboxylic groups) and DI water and centri- fuged at 5000 rpm several times. Resultant product was dried at 60 °C in an oven.

Reduction of GO using L-citrulline $(rGO)_2$

As-synthesized 20 mg GO was added into 80 mL DI water and sonicated for 2 h until to make it completely soluble. L-Citrulline (70 mg, 2 mM) was added into homogenous GO solution and stirred for 2 h at 80 °C (Wang et al. 2017). The mixture was cooled down at RT and centri- fuged with NaOH (1 M) first and then with DI water sev- eral times at 5000 rpm. After washing, the resultant prod- uct was dried in an oven at 60 °C. A pictorial diagram shown in Fig. 1 represents the synthesis of GO, $(rGO)_1$ and $(rGO)_2$ stepwise.

Thin-film formation

Thin films of GO, $(rGO)_1$, and $(rGO)_2$ were deposited on a glass substrate using spin-coating method. The glass sub- strates were cleaned by standard cleaning method (using acetone, de-ionized water, aqua regia, and isopropanol). For the deposition of film on glass substrate, solution of as-synthesized samples (1 mg/mL) with ethylene glycol was prepared under continuous sonication for 2 h. Spin-coating method was used for deposition with 600 rpm spin rate for 2 min. This process was repeated three times, and after every step, samples were dried at 60 °C to obtain GO, $(rGO)_1$, and $(rGO)_2$ films. Silver paste was used for contact formation. A stepwise flow diagram for the sensing device based on synthesized samples is shown in Fig. 2.

Instruments and characterizations

Synthesized GO, $(rGO)_1$, and $(rGO)_2$ were characterized with the help of Raman spectroscopy (STR 500 Confo- cal Micro Raman Spectrometer at 532 nm wavelength), Thermo-gravimetric Analysis (TGA; Perkin Elmer STA 6000 under N_2 environment), and X-ray diffraction (XRD; X-pert powder diffractometer using

copper rotating anode with incident beam of wavelength 1.54 Å). Surface struc- ture was characterized by field-emission scanning electron microscope (FESEM; NOVA nano SEM) and transmission

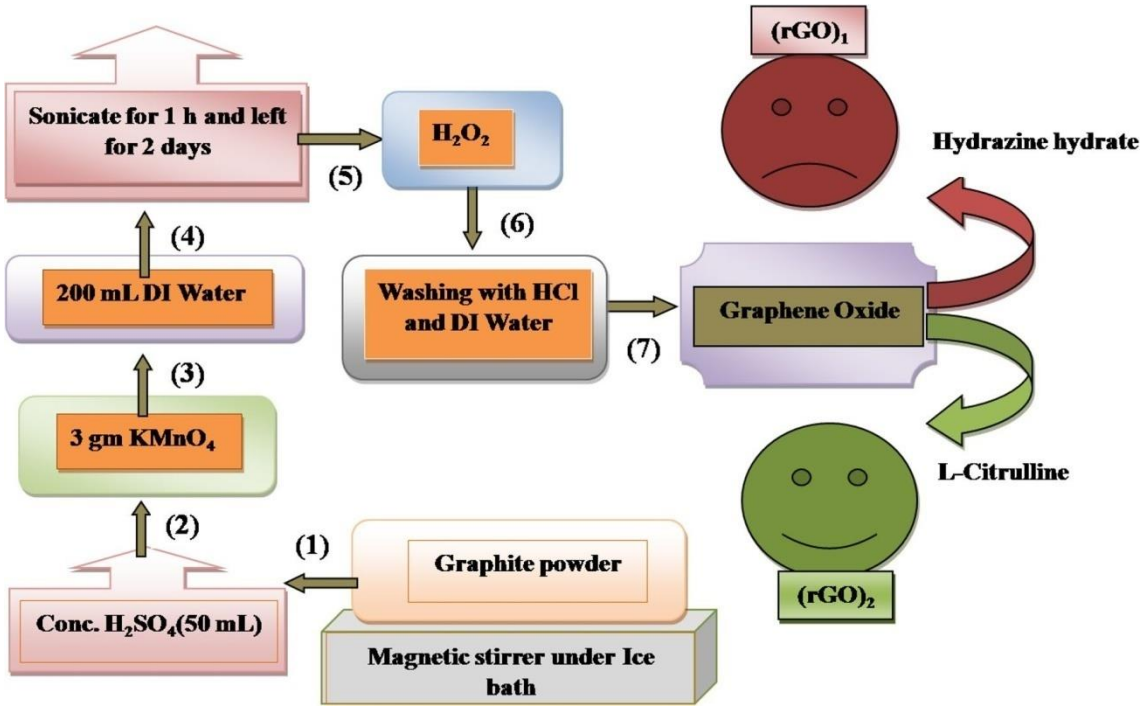

Fig. 1 Flowchart for preparation of GO (using Hummer's method), $(rGO)_1$ (using hydrazine hydrate), and $(rGO)_2$ (using green-reducing agent L-citrulline)

electron microscopy (TEM-Technie G2 20 FEI with accel- erating voltage 200 kV). Functional groups were identified by Fourier transform infrared spectroscopy (FTIR; Perkin Elmer system under transmission mode using KBr salt). Gas-sensing measurements of samples were recorded by digital multimeter Keithley-2400 Source Meter controlled by LabVIEW™ 2010 software. Gas concentration of the test gas to be detected by the sample was controlled by mass flow controller (DFC26S-VADN5-C5A).

Fig. 2 Flow diagram for the gas sensor based on GO, $(rGO)_1$, and $(rGO)_2$

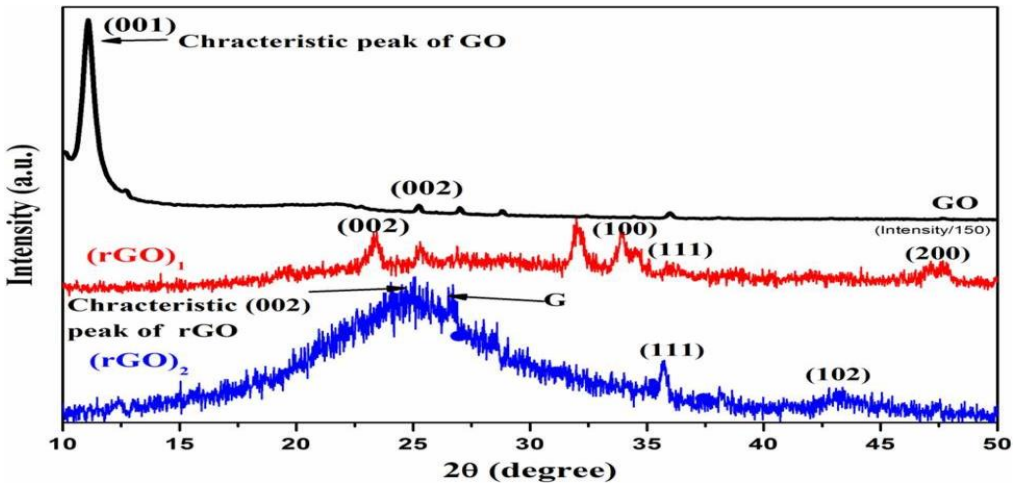

Fig. 3 XRD spectra of GO, hydrazine hydrate reduced GO, $(rGO)_1$, and L-citrulline reduced GO, $(rGO)_2$

Results and discussion

XRD study

RD patterns for GO and reduced GO [$(rGO)_1$ and $(rGO)_2$] are shown in Fig. 3. The diffraction pattern for GO exhibits a sharp diffraction peak at 11.07° which is indicative of dif- fraction from lattice plane (001) with *d*-spacing of 0.80 nm (Blanton et al. 2013a; Gupta et al. 2013). Larger *d*-spacing of GO (0.80 nm) as compared to that of graphite (0.34 nm) (Neha et al. 2012) peaks indicates the presence of oxygen functionalities which cooperate in hydration and exfoliation of graphene sheets in aqueous medium (Wang et al. 2017). A small peak present at 25.4° is attributed to (002) plane which suggests graphitic structure remaining in GO (Ain 2018). The presence of small additional peaks at positions 27.1, 28.8, and 36.5° suggests that GO layers may not be fully interconnected with oxygen atoms (Gao et al. 2010; Hsiao et al. 2010; Siburian et al. 2018).

Post-reduction of GO by hydrazine hydrate, the peak at lower 2θ gets dissolved and a new peak appears at 23.4° cor- responding to the characteristic (002) lattice plane of rGO with *d*-spacing of 0.38 nm for specimen $(rGO)_1$ (Sharma et al. 2017a, 2019c). The decrement in *d*-spacing from 0.80 to 0.38 nm indicates the removal of oxygen moieties and leading to reestablishment of sp^2 structure (Wang et al. 2017). Some other additional peaks also exist at 34.1°, 36.2°, and 47.3° corresponding to (100), (111), and (200) planes (Ha et al. 2011; Sharma et al. 2017a), respectively. A small peak at 25.6° confirms closed stacking of sheet in (rGO)1 (Alsharaeh et al. 2016), and the peak at 32.0° is indicative of residues of the reduction reaction byproducts.

Furthermore, the diffraction pattern of GO reduced by L-citrulline exhibits a hump with a certain peak at 24.4° with *d*-spacing of 0.36 nm which can be ascribed to the char- acteristic (002) lattice plane of rGO (Sharma et al. 2019a) along with another peak (G) at 26.6° revealing the signa- ture of presence of graphitic nature in $(rGO)_2$ (Blanton et al. 2013b). The overall diffraction pattern could be originating due to the contribution of three phases; amorphous $(rGO)_2$ (contributing to hump in the pattern), graphitic nature [peak G due to close stacking of $(rGO)_2$ layers], and crystalline $(rGO)_2$ [contributing to peaks from (111) and (102) dif- fraction planes] (Ha et al. 2011; Gupta et al. 2017). The amorphous hump also shows random picking of graphene sheet in rGO (Sharma et al. 2019a). After reduction with L-citrulline, *d*-spacing was observed 0.36 nm, which indi-cate the removal of oxygen functionalities. The variation of Decrement in interlayer *d*-spacing as $(rGO)_2 < (rGO)_1 <$ GO as 0.36 < 0.38 < 0.80 nm indicates successful reduction of GO.

Raman study

Figure 4a–c shows deconvoluted Raman spectra employing pseudo-Voigt fitting of synthesized samples recorded with visible excitation (532 nm), which is indicative of two prom- inent bands (D and G) of graphitic lattice. The position of D and G band with intensity ratio I_D/I_G exhibiting information about defect concentration in the specimen is computed and listed in Table 1. The table shows small decrease in I_D/I_G ratio for $(rGO)_2$ and $(rGO)_1$ as compared to GO. The defect healing post-reduction of graphene oxide is similar to the other reports (Moon et al. 2010; Muhammad et al. 2014). The decreased I_D/I_G ratio is a result of reduction of oxygen moieties in graphene oxide. Furthermore, a small deviation in the centers of D and G bands of $(rGO)_1$ and $(rGO)_2$ is also observed which must be due to the oxygen moieties. Further confirmation about removal of oxygen functional groups is described in FTIR analysis.

FTIR study

Figure 5 shows FTIR spectra of GO, $(rGO)_1$, and $(rGO)_2$. The FTIR spectrum for GO shows an absorption band at position 3412 cm^{-1} corresponding to stretching of

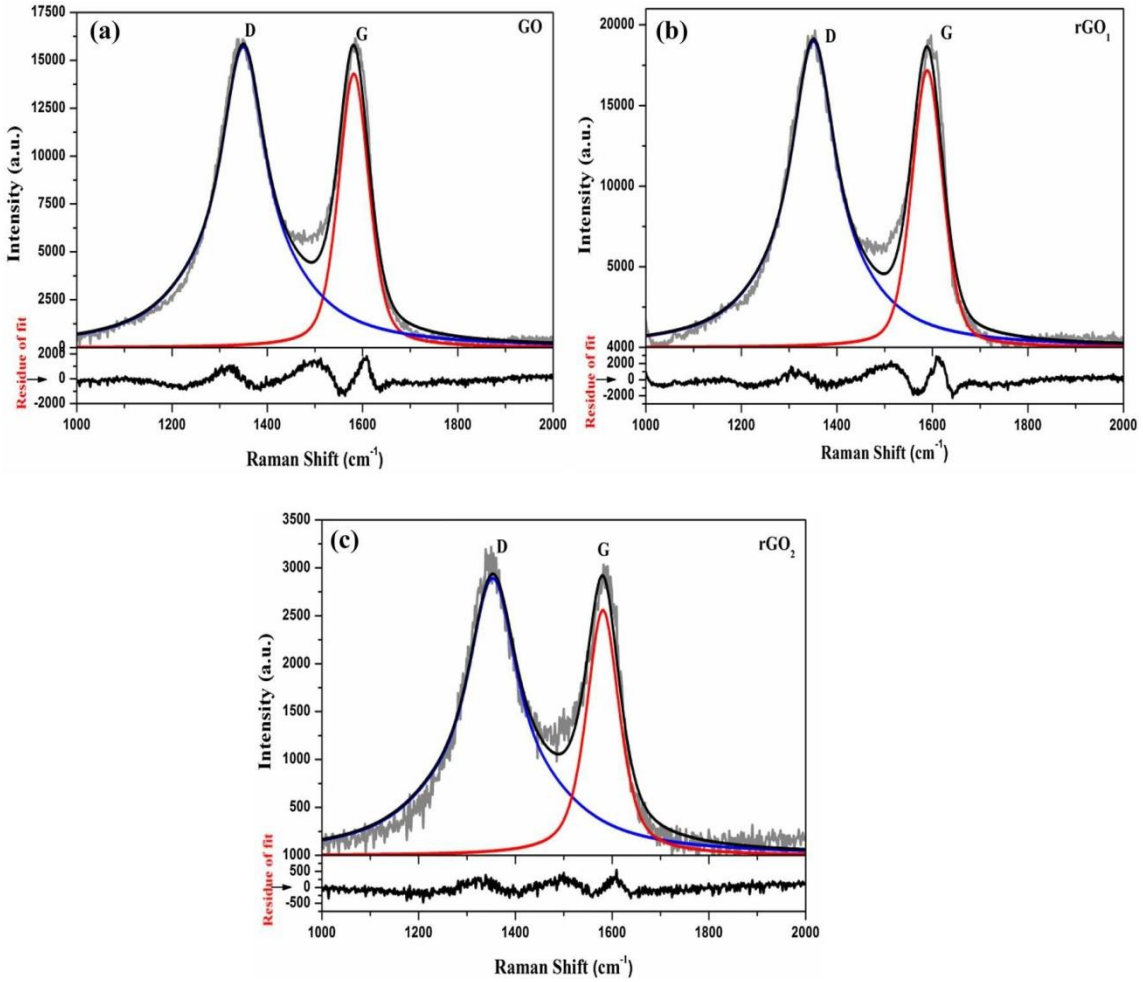

Fig. 4 Raman spectra of a GO, b hydrazine hydrate reduced GO, $(rGO)_1$, and c L-citrulline reduced GO, $(rGO)_2$

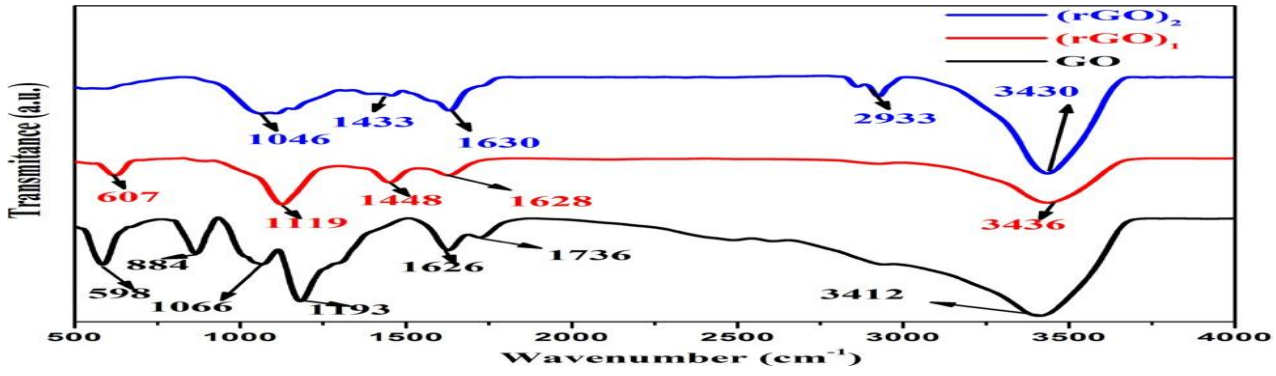

Fig. 5 FTIR spectra of GO, hydrazine hydrate reduced GO, $(rGO)_1$, and L-citrulline reduced GO, $(rGO)_2$. Removal of oxygen moieties indicates successfully reduction of GO

hydroxyl (–OH) group (Sharma et al. 2019b) and it shifts to 3436 cm^{-1} for $(rGO)_1$ and 3430 cm^{-1} for $(rGO)_2$. The broad absorption between 1620 and 1680 cm^{-1} is ascribed to stretching of alkene C=C as indicated for GO at 1626 cm^{-1}, $(rGO)_1$ at 1628 cm^{-1} and $(rGO)_2$ at 1630 cm^{-1} (Sharma et al. 2019b). The absorption band at around 1050–1200 cm^{-1} is due to stretching of alco- holic C–O group (Jeong et al.

2009). In FTIR spectra, C–O group peaks were obtained at position (1066 and 1193 cm^{-1}) for GO, 1119 cm^{-1} for $(rGO)_1$, and 1046 cm^{-1} for $(rGO)_2$ (Jin et al. 2014). The peak position for oxygen group C–O shifts to lower wavenumber with reduction which confirms the removal of oxygen moieties in $(rGO)_1$ and $(rGO)_2$ (Wang et al. 2017), although this peak inten- sity is very small for $(rGO)_2$ as compared to $(rGO)_1$. The peaks observed between 675 and 1000 cm^{-1} originate due to bending of =C–H (alkene) group. The =C–H group is present in GO at positions 598 and 884 cm^{-1} which is not seen in $(rGO)_2$. The FTIR spectra for $(rGO)_2$ show a peak at 1433 cm^{-1} which is attributed to stretching of aromatic C=C group (Sharma et al. 2019b). The presence of aro- matic C=C group suggests preservation of sp^2 carbons after reduction of GO with L-citrulline. A small peak at 2933 cm^{-1} indicates minute presence of alkane (C–H) group after reduction with L-citrulline (Du et al. 2019). In FTIR spectra, it is observed that reduction of GO with L-citrulline $(rGO)_2$ has small intensity of peaks due to oxygen functional groups concluding better reduction in $(rGO)_2$ as compared to that for $(rGO)_1$ (Fan et al. 2010; Wang et al. 2017). This supports the conclusions drawn from XRD and Raman studies.

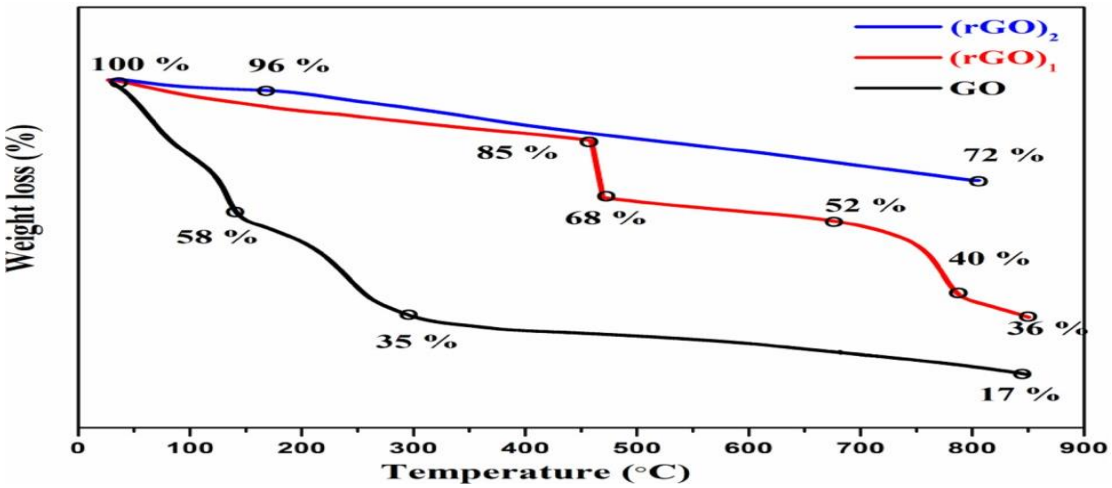

Fig. 6 TGA spectra of GO, hydrazine hydrate reduced GO, $(rGO)_1$, and L-citrulline reduced GO, $(rGO)_2$

TGA study

TGA spectra for GO and reduced GO are shown in Fig. 6. This measurement was carried out under N_2 flow of 20 mL/ min in temperature range 30–850 °C under heating rate of 20 °C/min. Weight loss for GO is observed at three instances in the given temperature range. First instance of weight loss is observed at 38–150 °C (~ 42%) attributed to the evapora- tion of absorbed water molecules (Dave et al. 2015) attached to GO grains by means of physisorption and chemisorption. The second instance (~ 25%) takes place in the tempera- ture range 190–275 °C due to the decomposition of oxygen functional groups. The last instance of weight loss (~ 8%) is observed at around 414 °C and ascribed to the presence of unstable carbon yielding CO_2 and CO (Loryuenyong et al. 2013; Sharma et al. 2017b). It is observed that weight loss in vicinity of 850 °C has become approximately constant indicating no further decomposition with temperature.The weight loss curve for $(rGO)_1$ indicates its first weight loss (~ 15%) at around 68 °C which is due to the releasing of water molecules which is continued till 450 °C indicating removal of stable oxygen Functionalities. During the tem- perature range 455–473 °C, a sudden weight loss (~ 17%) occurs which is due to scissioning of carbon bonds due to pyrolysis of carbon skeleton (Jeong et al. 2009). The next prominent weight loss of 12% is at around 730–

770 °C and 36% of sample $(rGO)_1$ remains at 850 °C temperature.The major weight loss (4%) for $(rGO)_2$ specimen occurs in temperature range 85–150 °C due to the release of water molecules (4%) and a continuous loss trend is seen up to 750 °C. At 797 °C, $(rGO)_2$ has a remaining weight of 72% as compared with $(rGO)_1$ and GO specimen. TGA shows smaller weight loss for $(rGO)_2$ 850 °C in comparison to that for $(rGO)_1$ and GO due to higher removal of oxygen functional groups (shown by FTIR). This suggests $(rGO)_2$ to have higher thermal stability than GO and $(rGO)_1$, which may lead to better graphitization (Fahrul et al. 2015).

FESEM study

Field-emission scanning electron microscope exposes the details of morphology and structure of GO, $(rGO)_1$ and $(rGO)_2$ specimens in their powder form as shown in Fig. 7. The FESEM image of GO shown in Fig. 7a indicates well- defined wrinkled sheets structure stacked on top of one another while fig 7b indicates colescaled winckled sheets with fragments of the same scattered in the whole scan area. The surface morphology of $(rGO)_2$ shown in Fig. 7c is similar to the surface morphology shown by GO in Fig. 7a, albeit, the wrinkled sheet structure seems relatively open containing less number of layers contributing to the sheet (Sharma et al. 2019a). The relatively open structure exhib- ited by $(rGO)_2$ provides more adsorption sites and better diffusion of test gas molecules which is essential for reali- zation of a better gas sensor (Katkov et al. 2014). TEM results as shown in Fig. 8 provide more information about the microstructure.

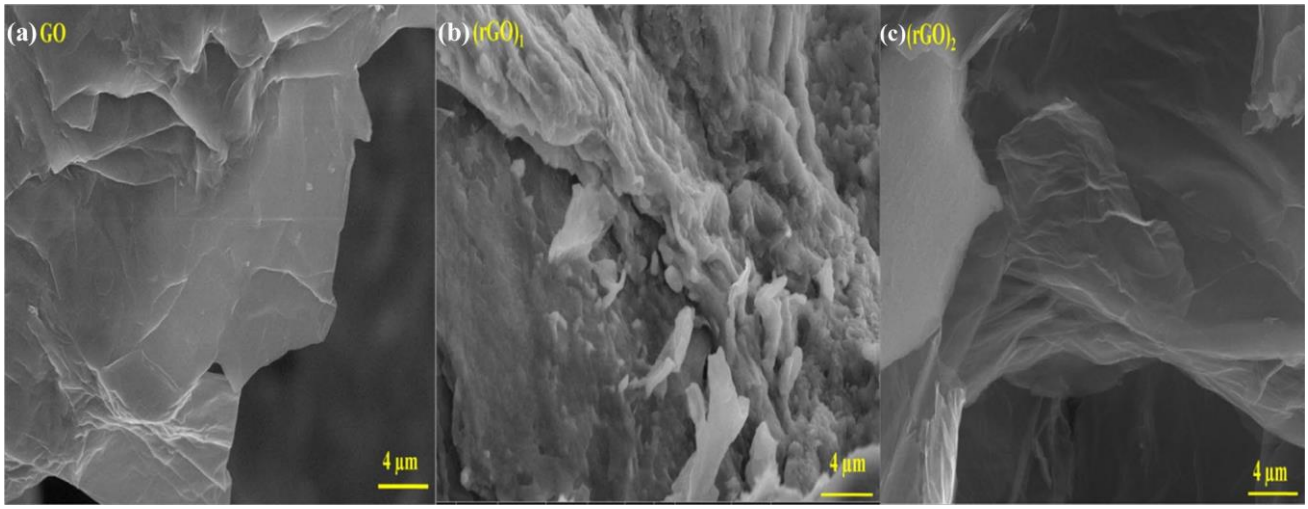

Fig. 7 FESEM images a GO, b hydrazine hydrate reduced GO, $(rGO)_1$, and c L-citrulline reduced GO, $(rGO)_2$. Wrinkled sheet structure of syn- thesized samples makes them suitable for gas-sensing properties

TEM STUDY

Figure 8a, b shows the TEM images of GO, $(rGO)_1$, and $(rGO)_2$ and corresponding selected area electron diffrac- tion (SAED) in their inset. TEM images of synthesized samples show wrinkled sheet structure of GO as well as $(rGO)_1$ and $(rGO)_2$. TEM image of $(rGO)_1$ shows the lay- ers to be closely stuck together, while $(rGO)_2$ is more transparent in comparison to GO and $(rGO)_1$ as observed in FESEM also. The SAED pattern (shown in the inset) of GO, $(rGO)_1$, and $(rGO)_2$ is supported with XRD results.

Sensing measurements

It is evident from the studies carried out that GO, $(rGO)_1$, and $(rGO)_2$ qualify the basis for realization of a gas sen- sor. These films were employed for NO_2 gas sensing by sourcing a voltage of 4 V and measurement of current/ resistance through Ag contacts resting on the film. The exposure for test gases was done at a

constant flow rate of 30 sccm with a balanced gas a mixture of (N_2 + O_2). Multiple NO_2 gas exposure was given to specimen for testing the repeatability of measurements (shown in Fig. S1 in supplementary file) and the summary of such results is given in the gas-sensing curves provided as Figs. 9 and 10.

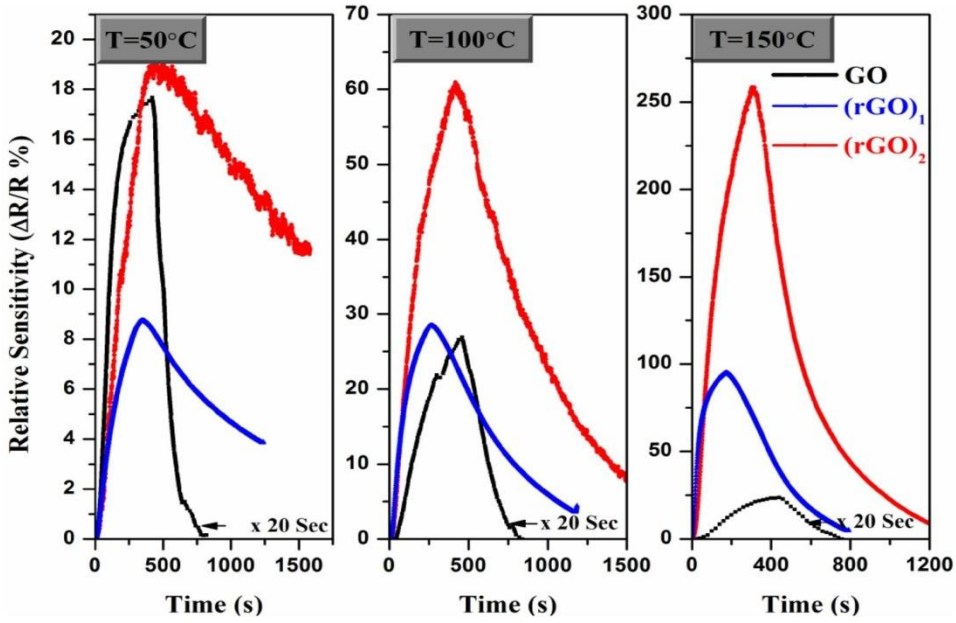

Fig. 9 Relative sensitivity of GO/(rGO)1 and (rGO)2 for 10 ppm NO_2 at operating temperature of 50 °C, 100 °C, and 150 °C

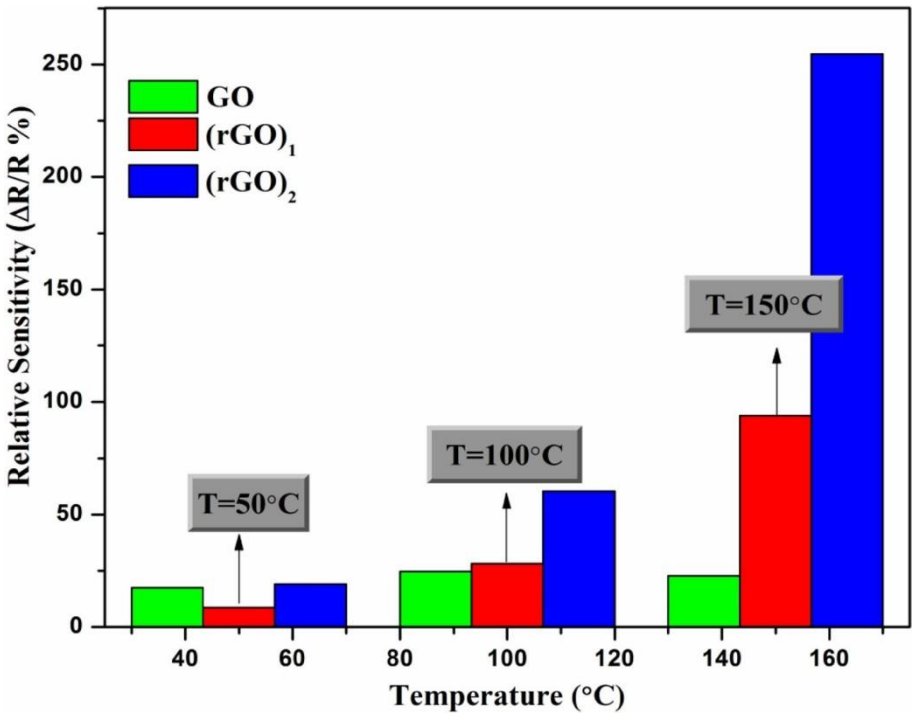

Fig. 10 Histogram of Relative sensitivity of GO/(rGO)$_1$ and (rGO)$_2$ versus temperature for 10 ppm NO_2

Gas-sensing characteristic curves are represented in Figs. 9 and 10 for 10 ppm NO_2 gas exposure at operating tempera-tures of 50 °C, 100 °C, and 150 °C. An anomalous effect is observed on exposure of NO_2 gas in all of these specimens. GO, (rGO)$_1$, and (rGO)$_2$ normally offer p-type electrical properties and exposure of an

oxidizing gas should decrease their resistance. However, the exposure increased the resistance of the specimen in the current study and has not been reported earlier for GO/rGO. This indicates switching of these normally p-type materials to n-type materials on exposure to NO_2. This may be due to when gas sensor exposed by NO_2, $NO_{2,ads}$ will not only replace the $O_{,ads}$, but also lead to the surface adsorbed active sites redistribution. As the distance between $NO_{2,ads}$ and $O_{,ads}$ is shorter, so they can interact with the manner of below equation. Capturing of electron from film increases sensor resistance which indicates switching of p-type to n-type (Dai et al. 2015):

This phenomenon has earlier been reported in case of metal-oxide gas sensors (Gurlo et al. 2004; Siciliano et al. 2009; Vyas et al. 2013) and attributed to the formation of an inversion-type surface charge region (Sberveglieri 2008) which offers a switching of n-type to p-type switching to the bulk of specimen.

The gas-sensing characteristic curves are indicative of increased gas sensitivity post-reduction which is an obvi- ous result due to availability of oxygen dangling bonds in $(rGO)_1$ and $(rGO)_2$. Better gas-sensing properties of $(rGO)_2$ with respect to $(rGO)_1$ for all operating temperature is due to higher defect concentration in $(rGO)_2$, a fact well cor- roborated by XRD and Raman studies. These defect states are known to act as preferential adsorption sites for NO_2 (Ahn et al. 2008).

The conductivity switching in these specimens are pro- nounced due to high signal-to-noise ratio at all operating temperatures which indicates stability of inversion layer in the given temperature range. This type of effect is of impor- tance in gas-sensing studies, since it entails a unique phe- nomenon for a selective gas. A histogram of relative sensitivity versus temperature for 10 ppm NO_2 of GO/$(rGO)_1$ and $(rGO)_2$ shown in Fig. 10. Figure 10 indicates relative sensitivity of green-synthesized $(rGO)_2$; 254.7% at 150 °C, 60.3% at 100 °C and 19.1% at 50 °C higher than that of $(rGO)_1$; 93.9% at 150 °C, 28.3% at 100 °C, 8.7% at 50 °C and GO; 22.7%, 24.8%, 17.5% at 150, 100, 50 °C, respectively.

To establish better sensitivity of recent green-synthesized rGO, $(rGO)_2$ than rGO synthesized by chemical reduc- ing agents or by other methods, we have gathered sens- ing data from the published literature and listed them in Table 2. However, it would be difficult to make a compari- son between published reports and the current study as no reports could be found for response of NO_2 gas for similar concentration and temperature. From Table 2, it is clear that response of gas-sensing device based on green-synthesized rGO—$(rGO)_2$ is better than already published results. In this table, a green-synthesized rGO (by caffeic acid) is also listed which shows smaller response than our green-synthesized rGO. So here, we can say that $(rGO)_2$ reduced by L-citrul- line is an effective gas-sensing material giving higher gas- sensing performance and environment friendly as well. In addition, these synthesized products were also used to test 10 ppm CO gas at the same temperatures as for NO_2 and the obtained results are given in Fig. S2 in supplementary file.

Conclusion

Here, we report a comparison study for gas-sensing measure- ments of reduced graphene oxide (rGO) synthesized through chemical and green method. Graphene oxide was prepared by oxidation of graphite flakes using Hummer's method and then reduced with (1) hydrazine hydrate giving $(rGO)_1$ and (2) L-citrulline giving $(rGO)_2$. The *d*-spacing obtained from XRD pattern was 0.36 nm for $(rGO)_2$; lesser than that of $(rGO)_1$ and GO, which are 0.38 nm and 0.80 nm, respec- tively. XRD and FTIR confirm the synthesis of GO by intro- duction of oxygen functionalities such as (–OH) hydroxyl and (–COOH) carboxylic, and also confirm its reduction to rGO by hydrazine hydrate and L-citrulline shown byremoval of these oxygen functional groups. Raman spectros- copy shows decreased I_D/I_G ratio for rGO

[$(rGO)_2$ = 0.891, $(rGO)_1$ = 0.897 and for GO as 0.904], which confirm reduc- tion of oxygen moieties in case of rGO and also presence of defects for the same. TGA results for $(rGO)_2$ show smaller percentage of weight loss 28% in comparison to that for $(rGO)_1$ which has higher amount of weight loss (64%) at 800 °C. Surface morphology of prepared samples seen with FESEM and TEM reveals porous nanosheet morphology with lesser number of layers for $(rGO)_2$. Synthesized prod- ucts were tested for 10 ppm NO_2 gas at temperature of 50, 100, and 150 °C. The investigation shows $(rGO)_2$ as sensor giving maximum response of ~ 254.7% for NO_2 at 150 °C. Interestingly, a switching of p-type synthesized materials [GO, $(rGO)_1$ and $(rGO)_2$] to n-type was observed on expo- sure to NO_2 gas. These results show that green-synthesized $(rGO)_2$ is more selective for NO_2 gas. The characteristics of green-reduced rGO in terms of its morphology, thermal stability, and gas-sensing results show it to be a potential material for gas sensing and are a motivation to develop a consistent method for the production of reduced graphene oxide without causing any harm to the environment.

References

1. Ahn MW, Park KS, Heo JH et al (2008) Gas sensing properties of defect-controlled ZnO-nanowire gas sensor. Appl Phys Lett 93:2008–2010. https://doi.org/10.1063/1.3046726
2. Ain QT (2018) Effect of solvents on optical band gap of silicon- doped graphene oxide. Mater Res Express. https ://doi. org/10.1088/2053-1591/aab239
3. Alsharaeh E, Ahmed F, Aldawsari Y, Khasawneh M (2016) Novel synthesis of holey reduced graphene oxide (HRGO) by micro- wave irradiation method for anode in lithium-ion batteries. Nat Publ Gr. https://doi.org/10.1038/srep29854
4. Anh T, Sik J, Su J, Tae Y (2011) Colloids and surfaces a: phys- icochemical and engineering aspects one-step reduction of graphene oxide with L-glutathione. Colloids Surf A Physico- chem Eng Asp 384:543–548. https://doi.org/10.1016/j.colsu rfa.2011.05.019
5. Blanton TN, Majumdar D, Company EK (2013a) This document was presented at the Denver X-ray Conference (DXC) on applications of X-ray analysis. Sponsored by the International Centre for Dif- fraction Data (ICDD). This document is provided by ICDD in cooperation with the authors and presenters of
6. Blanton TN, Majumdar D, Company EK (2013b) Characterization of X-ray irradiated graphene oxide coatings using X-ray diffraction, X-ray photoelectron spectroscopy, and atomic force microscopy 56
7. Bo Z, Shuai X, Mao S et al (2014) Green preparation of reduced gra- phene oxide for sensing and energy storage applications. Sic Rep. https://doi.org/10.1038/srep04684
8. Chen K, Ling Y, Cao C et al (2016) Chitosan derivatives/reduced graphene oxide/alginate beads for small-molecule drug deliv- ery. Mater Sci Eng C 69:1222–1228. https://doi.org/10.1016/j.msec.2016.08.036
9. Dai Z, Lee CS, Tian Y et al (2015) Highly reversible switching from P- to N-type NO_2 sensing in a monolayer Fe_2O_3 inverse opal film and the associated P–N transition phase diagram. J Mater Chem A 3:3372–3381. https://doi.org/10.1039/c4ta05438e
10. Dai M, Zhao L, Gao H et al (2017) Hierarchical assembly of α-Fe_2O_3 nanorods on multiwall carbon nanotubes as a high-performance sensing material for gas sensors. ACS Appl Mater Interfaces. https://doi.org/10.1021/acsami.7b00805
11. Dave K, Park KH, Dhayal M (2015) Two-step process for program- mable removal of oxygen functionalities of graphene oxide :functional, structural and electrical characteristics. RSC Adv. https://doi.org/10.1039/c5ra18880f

12. Du Y, Khan S, Zhang X et al (2019) In situ preparation of porous car- bon nanosheets loaded with metal chalcogenides for a superior oxygen evolution reaction. Carbon N Y 149:144–151. https://doi.org/10.1016/j.carbon.2019.04.048
13. Eda G, Fanchini G, Chhowalla M (2008) Large-area ultrathin films of reduced graphene oxide as a transparent and flexible electronic material. Nat Nanotechnol 3:270–274. https://doi.org/10.1038/nnano.2008.83
14. Fahrul M, Hanifah R, Jaafar J, Aziz M (2015) Effects of reduction time on the structural, electrical and thermal properties of synthesized reduced graphene oxide nanosheets. Bull Mater Sci 38:1569–1576
15. Fan Z, Wang K, Wei T et al (2010) An environmentally friendly and efficient route for the reduction of graphene oxide by aluminum powder. Carbon N Y 48:1686–1689. https://doi.org/10.1016/j.carbon.2009.12.063
16. Fernández-Merino MJ, Guardia L, Paredes JI et al (2010) Vitamin C is an ideal substitute for hydrazine in the reduction of graphene oxide suspensions. J Phys Chem C 114:6426–6432. https://doi.org/10.1021/jp100603h
17. Gao X, Jang J, Nagase S (2010) Hydrazine and thermal reduction of graphene oxide : reaction mechanisms, product structures, and reaction design. J Phys Chem C 114(2):832–842
18. Ghosh A, Late DJ, Panchakarla LS et al (2009) NO_2 and humidity sensing characteristics of few-layer graphenes. J Exp Nanosci 4:313–322. https://doi.org/10.1080/17458080903115379
19. Gong Z, Karandikar S, Zhang X, et al (2010) Composite nanomaterial thin film-based biosensors. SENSORS, IEEE, Kona, HI, pp 29–32
20. Guo L, Hao Y-W, Li P-L et al (2018) Improved NO_2 gas sensing prop- erties of graphene oxide reduced by two-beam-laser interference. Sci Rep 8:4918. https://doi.org/10.1038/s41598-018-23091-1
21. Gupta RK, Alahmed ZA, Yakuphanoglu F (2013) Graphene oxide based low cost battery. Mater Lett 112:75–77. https://doi. org/10.1016/j.matlet.2013.09.011
22. Gupta B, Kumar N, Panda K et al (2017) Role of oxygen functional groups in reduced graphene oxide for lubrication. Nat Publ Gr. https://doi.org/10.1038/srep45030
23. Gurlo A, Bârsan N, Oprea A et al (2004) An n- to p-type conductivity transition induced by oxygen adsorption on α-Fe_2O_3. Appl Phys Lett 85:2280–2282. https://doi.org/10.1063/1.1794853
24. Ha H, Kim Y, Hwang S, Ruoff RS (2011) One-pot synthesis of plati- num nanoparticles embedded on reduced graphene oxide for oxy- gen reduction in methanol fuel cells. Electrochem Solid State Lett 14:73–76. https://doi.org/10.1149/1.3584092
25. Hsiao M, Liao S, Yen M et al (2010) Preparation of covalently func- tionalized graphene using residual oxygen-containing functional groups. ACS Appl Mater Interfaces. https://doi.org/10.1021/am100597d
26. Huang C, Li C, Shi G (2012) Graphene based catalysts. Energy Environ Sci 5:8848. https://doi.org/10.1039/c2ee22238h
27. Jeong H, Lee YP, Jin MH et al (2009) Thermal stability of graphite oxide. Chem Phys Lett 470:255–258. https://doi.org/10.1016/j. cplett.2009.01.050
28. Jeong HY, Lee D, Choi HK et al (2012) Flexible room-temperature NO_2 gas sensors based on carbon nanotubes/reduced graphene hybrid films flexible room-temperature NO_2 gas sensors based on
29. carbon nanotubes/reduced graphene hybrid films. Appl Phys Lett 213105:2010–2013. https://doi.org/10.1063/1.3432446

30. Jin L, Yue D, Xu Z et al (2014) RSC advances reinforced nano fiber mats. RSC Adv 4:35035–35041. https://doi.org/10.1039/C4RA03987D
31. Jin L, Li J, Liu L et al (2018) Facile synthesis of carbon dots with superior sensing ability. Appl Nanosci. https://doi.org/10.1007/s13204-018-0755-3
32. Katkov MV, Song H, Okotrub AV, Bulusheva G (2014) Wrinkled reduced graphene oxide nanosheets for highly sensitive and easy recoverable NH 3 gas detector. RSC Adv 4:46930–46933. https://doi.org/10.1039/C4RA08811E
33. Ko G, Kim H, Ahn J et al (2010) Graphene-based nitrogen dioxide gas sensors current (μA). Curr Appl Phys 10:1002–1004. https://doi. org/10.1016/j.cap.2009.12.024
34. Liu Y, Dong X, Chen P (2012) Biological and chemical sensors based on graphene materials. Chem Soc Rev 41:2283–2307. https://doi. org/10.1039/C1CS15270J
35. Liu S, Yu B, Zhang H et al (2014) Enhancing NO_2 gas sensing perfor- mances at room temperature based on reduced graphene oxide- ZnO nanoparticles hybrids. Sens Actuators B Chem 202:272–278. https://doi.org/10.1016/j.snb.2014.05.086
36. Loryuenyong V, Totepvimarn K, Eimburanapravat P, et al (2013) Prep- aration and characterization of reduced graphene oxide sheets via water-based exfoliation and reduction methods. Adv Mater Sci Eng. https://doi.org/10.1155/2013/923403
37. Moon IK, Lee J, Ruoff RS, Lee H (2010) Reduced graphene oxide by chemical graphitization. Nat Commun 1:1–6. https://doi. org/10.1038/ncomms1067
38. Muhammad S, Ritikos R, James T et al (2014) A practical carbon diox- ide gas sensor using room-temperature hydrogen plasma reduced graphene oxide. Sens Actuators B Chem 193:692–700. https://doi. org/10.1016/j.snb.2013.12.017
39. Neha B, Manjula KS, Srinivasulu B, Subhas SC (2012) Synthesis and characterization of exfoliated graphite/ABS composites. Open J Org Polym Mater 2012:74–78
40. Online VA, Mahbubul IM, Rahman S, Metselaar HSC (2016) The green reduction of graphene oxide. RSC Adv. https://doi. org/10.1039/C6RA03189G
41. Robinson JT, Perkins FK, Snow ES et al (2008) Reduced graphene oxide molecular sensors. Nano Lett 8:3137–3140. https://doi. org/10.1021/nl8013007
42. Sberveglieri G (ed) (2008) Solid state gas sensing. Springer, Berlin Sharma N, Sharma V, Jain Y et al (2017a) Synthesis and charac-
43. terization of graphene oxide (GO) and reduced graphene oxide (rGO) for gas sensing application. Macromol Symp. https://doi. org/10.1002/masy.201700006
44. Sharma V, Jain Y, Kumari M et al (2017b) Synthesis and charac- terization of graphene oxide (GO) and reduced graphene oxide (rGO) for gas sensing application. Macromol Symp. https://doi. org/10.1002/masy.201700006
45. Sharma N, Sharma V, Sharma SK, Sachdev K (2019a) Gas sensing behaviour of green synthesized reduced graphene oxide (rGO) for H_2 and NO. Mater Lett. https://doi.org/10.1016/j.matle t.2018.10.145
46. Sharma N, Sharma V, Sharma SK, Sachdev K (2019b) Gas sensing behaviour of green synthesized reduced graphene oxide (rGO) for H_2 and NO. Mater Lett 236:444–447. https://doi.org/10.1016/j. matlet.2018.10.145
47. Sharma N, Sharma V, Vyas R et al (2019c) A new sustainable green protocol for production of reduced graphene oxide (rGO) and its gas sensing properties. J Sci Adv Mater Devices. https://doi. org/10.1016/j.jsamd.2019.07.005

48. Siburian R, Sihotang H, Raja SL et al (2018) New route to synthesize of graphene nano sheets. Orient J Chem. https://doi.org/10.13005/ojc/340120
49. Siciliano T, Tepore A, Micocci G et al (2009) Transition from n- to p-type electrical conductivity induced by ethanol adsorption on α-tellurium dioxide nanowires. Sens Actuators B Chem 138:207–213. https://doi.org/10.1016/j.snb.2009.02.007
50. Singh V, Joung D, Zhai L, Das S (2011) Progress in materials science graphene based materials: past, present and future. Prog Mater Sci 56:1178–1271. https://doi.org/10.1016/j.pmatsci.2011.03.003
51. Su P, Shieh H (2014) Flexible NO_2 sensors fabricated by layer-by-layer covalent anchoring and in situ reduction of graphene oxide. Sens Actuators B 190:865–872
52. weet D (2015) Oh, the places you'll go with your Ph.D.! Cell 163:1304–1305. https://doi.org/10.1016/j.cell.2015.11.016
53. Tian W, Liu X, Yu W (2018) Progress of gas sensor based on gra- phene and its derivatives: a review. Appl Sci Res. https://doi. org/10.3390/app8071118
54. Varghese SS, Lonkar S, Singh KK et al (2015) Recent advances in gra- phene based gas sensors. Sens Actuators B Chem 218:160–183. https://doi.org/10.1016/j.snb.2015.04.062
55. Vyas R, Sharma S, Gupta P et al (2013) Nitrogen dioxide induced con- ductivity switching in ZnO thin film. J Alloys Compd 571:6–11. https://doi.org/10.1016/j.jallcom.2013.03.217
56. Wang J, Caliskan E, Lidija Š (2017) Green reduction of graphene oxide using alanine. Mater Sci Eng C 72:1–6. https://doi.org/10.1016/j. msec.2016.11.017
57. Wu J, Tao K, Miao JM, Norford L (2015) Improved selectivity and sen- sitivity of gas sensing using 3D reduced graphene oxide hydrogel with integrated microheater School of Mechanical and Aerospace Engineering, Nanyang Technological University, Center for Envi- ronmental Sensing and Modeling (CENSAM), Singapore-MIT Alliance for. ACS Appl Mater Interfaces. https://doi.org/10.1021/ acsami.5b09695
58. Xue N, Zhang Q, Zhang S et al (2017) Highly sensitive and selec- tive hydrogen gas sensor. Sensor 2:1–17. https://doi.org/10.3390/ s17102351
59. Yang S, Jiang C, Wei S (2017) Gas sensing in 2D materials. Appl Phys Rev. https://doi.org/10.1063/1.4983310
60. Ye W, Li X, Luo J et al (2017) Industrial crops & products lignin as a green reductant and morphology directing agent in the fabrication of 3D graphene-based composites for high-performance superca- pacitors. Ind Crop Prod 109:410–419. https://doi.org/10.1016/j. indcrop.2017.08.047
61. Yoon HJ, Jun DH, Yang JH et al (2011) Carbon dioxide gas sensor using a graphene sheet. Sens Actuators B Chem 157:310–313. https://doi.org/10.1016/j.snb.2011.03.035
62. Zhang Y, Tan YW, Stormer HL, Kim P (2005) Experimental observa- tion of the quantum Hall effect and Berry's phase in graphene. Nature 438:201–204. https://doi.org/10.1038/nature04235
63. Zhezhe W, Shang H, Zhao R, Xing X, Wang Y (2017) ZnO nanoparti- cles as sensing materials with high gas response for detection of *n*-butanol gas. J Nanostruct 7:103–110. https://doi.org/10.22052/jns.2017.02.003